Effect of a novel pin tool with shoulder at the top of the needle on the formability, microstructure and properties of Al/Mg dissimilar friction stir lap joint

Tianfan Jiang
Jinpeng Hu
Yifu shen (yfshen_nuaa@hotmail.com)
Nanjing University of Aeronautics and Astronautics https://orcid.org/0000-0002-7162-262X
Tao Sun
Ruiyang Ni
Fujun Cao
Tao Yu
Guangming Zhou

Research Article

Keywords: Friction stir lap welding, Aluminum alloy, Magnesium alloy, Dissimilar materials joining

Posted Date: November 22nd, 2022

DOI: https://doi.org/10.21203/rs.3.rs-2282582/v1

Version of Record: A version of this preprint was published at The International Journal of Advanced Manufacturing Technology on January 23rd, 2024. See the published version at https://doi.org/10.1007/s00170-024-12970-9.

Abstract

In this paper, a novel friction stir welding tool with shoulder at the top of the needle is developed to solve the problems in aluminum/magnesium friction stir lap welding. Based on the structural design of the shoulder at the end of the needle, the temperature difference in the thickness direction of the joint was coordinated, and the aluminum-magnesium dissimilar lapping joint was successfully prepared in two kinds of lapping methods. Taking die cast AZ31B magnesium alloy and extruded 6061 aluminum alloy as the research object, the defects and microstructure of weld joint were observed and analyzed by optical microscope and scanning electron microscope. Additionally, their mechanical properties were also evaluated. The results show that a good metallurgical reaction is formed between aluminum and magnesium, and with the increase of the effective plate thickness and the decrease of the effective lap width, the unique hook defect shape of lap welding is optimized, which also promotes the improvement of the mechanical properties of the weld. In the tensile shear experiment, it is found that the tensile shear property is improved due to the change of the shape of the hook defect, and it is a mixed fracture of toughness and brittleness.

Introduction

In recent years, with the deepening of the concept of energy conservation and environmental protection in the world, the requirements for lightweight products in the industrial field are also getting higher and higher. The proportion of traditional high-density materials is gradually reduced, and replaced by low-density materials[1].As a representative of light metals, aluminum alloy and magnesium alloy have high specific strength, specific stiffness, corrosion resistance and other advantages, which are widely used in aerospace and automotive industries[2, 3]. Therefore, it is inevitable to realize the dissimilar welding of light aluminum and magnesium metals.

When aluminum-magnesium alloys are welded by traditional welding procedure, it is easy to form defects such as pores and thermal cracks in the joint due to the large difference between the physical and chemical properties of the two. Moreover, it can be found from the Al-Mg phase diagram that the eutectic reaction temperature of aluminum-magnesium is low, and intermetallic compounds are easy to form in the joint[4, 5].Not only in the traditional arc welding, but also in the laser welding with high energy density and high cooling rate, the formation of intermetallic phase due to the high temperature deteriorates the joint property of the weld[6]. Therefore, to realize the connection of Al-Mg dissimilar alloys, it is necessary to control the heat input during the welding process, so as to reduce the formation of intermetallic compounds. As a kind of green solid phase welding, the welding temperature of friction stir welding is lower than the absolute melting temperature of the welded alloy. Friction stir welding (FSW) is a relatively new solid-state welding technology invented by British Welding Institute (TWI) in 1991[7]. Wentao Hou et al[8].has realized solid connection and mechanical lock between interfaces through non-consumable rotating pin tool. Friction stir welding can avoid metallurgical defects caused by fusion welding and is more suitable for welding aluminum/magnesium dissimilar alloy[9].

At present, the research of aluminum-magnesium dissimilar friction stir lap welding (FSLW) is mainly realized by the traditional single-axial shoulder pin tool. VAHID, FIROUZDOR et al.[10] found that cracks can be observed in the center of the joint when 6061 aluminum alloy is used as the upper plate, and this crack has a significant impact on the tensile properties of the joint .Chen Y C et al.[11] found that when using single shoulder for lap welding of aluminum plate above magnesium plate, the smaller the welding speed (20mm/min),the less likely cracks will appear in the welding core area and transition area, and the mechanical properties of the weld will be improved. Mohammadi J et al.[12] performed lap welding of aluminum-magnesium dissimilar alloy with a conical stir needle with single axial shoulder thread, and found that when AZ31B was placed above Al 6061,the materials at the bottom of the weld core were mixed inhomogeneous and segregation occurred due to the different viscosity of aluminum-magnesium itself and the temperature required for forming eutectic structure. Ji S et al.[13] studied the lap welding of external stationary single axial shoulder, and found that although the lap joints with smooth surface and very small flash could be obtained, the hook defect at the interface of friction stir lap welding joint and the hole formed at the bottom of the weld could not be avoided, and the hook of Mg/Al joint was higher than that of Al/Mg joint.AS for hook defects, they believe that the mixing degree of RS side is better than that of AS side, and the flow performance of aluminum alloy is better than that of magnesium alloy.

In addition to cracks, holes and hook defects, the biggest problem of aluminum-magnesium dissimilar welding is that, due to the low eutectic temperature of aluminum-magnesium, intermetallic compounds are easily formed at the interface during the welding process, which is often the cause of fracture. Based on this perspective, in order to improve the performance of welded joints, S. Tan et al.[14] improved the mechanical properties of joints by reducing the thickness and distribution of intermetallic compounds. Liu Z et al.[15] and Lv et al.[16] found that with the assistance of ultrasound, the vibration and sound flow caused by ultrasound broke the continuous intermetallic compounds (IMCs) layer near the thermal-mechanical influence zone on the forward side into fragments or particles, and the mechanical interlocking was strengthened, thus improving the mechanical properties of the joint. Some scholars Farahani M S[17] and B Zheng[18] proposed to add zinc, tin and other metals to the lap interface as preset interlayer, and then carry out friction stir welding. The thermo-mechanical effect of the stirring tool on the interlayer and the matrix is used to promote the alloying reaction between the base material and the sandwich in the interface area, thus improving the effective interface connection area. The interlayer must be selected according to the specific base material type, which limits the type of weldable materials and the application field of this technology to a certain extent.

In summary, although the formation mechanism of defects in FSLW joint of single shoulder pin tool, the evolution mechanism of microstructure during welding, the types of IMCs and process optimization have been systematically studied, hook defects formed on the forward and retreating side (RS) and the formation of IMCs still cannot be completely avoided. Friction stir welding is essentially a combination of mechanical and thermal processes, both of which depend heavily on the interaction between the tool and the workpiece, directly determining the flow of the material and the heat generated. The bonding mechanism of friction stir welding depends on the recrystallization of the material in the stir zone.

Therefore, the stirring tool is the key factor of friction stir welding[8].Bandi et al.[5] studied the microstructure and properties of FSLW joints by changing the length of the stirring needle. They found that the depth of the stirring needle into the lower plate was directly proportional to the degree of mixing of the material at the core of the molten zone. That is to say, under the action of 4.25mm stirring needle, the material has better fluidity in the molten core area. It also promotes the dispersion of intermetallic compounds at the interface and improves the performance of the joint. This indicates that the shape of the pin tool itself has a significant influence on the lap interface.

Therefore, in this paper, starting from the overall structure of the pin tool, we design a pin tool whose end is similar to the shoulder. We expect to increase effective lap joint contact area, and the coordination of lap joint interface material liquidity by increasing the contact area between the pin tool and the lap surface of the lower plate. This can also solve the liquidity difference between dissimilar materials lead to the root defects, so as to improve the mechanical properties of joint.

Experimental Procedures

2.1 Experimental process

Friction stir welding of AA6061-T6 aluminum alloy and AZ31B magnesium alloy was carried out by lap welding method. Two lap welding methods were adopted, the first one was that the aluminum plate was located on the upper side of the magnesium plate (referred to as Al/Mg),and the second one was that the magnesium plate was located on the upper side of the aluminum plate (referred to as Mg/Al).In the welding process, the welding plate is fixed on the rigid workbench through the fixture, and then the welding speed (range from 20mm/min to 60mm/min),rotating speed (range from 700r/min to 1500r/min),spindle down pressure speed and constant spindle pressure amount (0.3mm) and other process parameters are set for automatic welding. Before welding, clean the surface of two kinds of plates to be welded to remove surface oxides. And then place the plates in the armor mode as shown in Fig. 1. During the welding process, the amount of lap between the two plates is controlled to be 60mm.The morphology and size of the pin tool used in the experiment are shown in Fig. 2. The shoulder at the end of the needle is defined as the shoulder of the needle top (abbreviated as SNT).

2.2 Experimental materials

The chemical compositions of matrix material (BM) 6061-T6 aluminum alloy and AZ31B magnesium alloy are shown in Tables 1 and 2, respectively. The size of the plate is 5mm×160mm×100mm, and the welding direction is perpendicular to the rolling direction of the plate. Fig. 2 is a schematic diagram of the size of the pin tool. The shoulder diameter of the pin tool is 18mm, the diameter of the needle is 6mm, the length is 5.5mm, and the diameter and height of the SNT are 8.5mm and 1.5mm. During the welding process, the SNT is controlled to be positioned on the lap interface. This design aims to widen the width of the effective lap interface, coordinate the flow of dissimilar metals at the interface, and improve the

adaptability of the pin tool. The whole tool is made of H13 steel, and its hardness is improved to 50 HRC after quenching and tempering. Its chemical composition is shown in Table 3.

Table 1 Main chemical composition of 6061-T6 aluminum alloy (mass fraction %)

Elements	Si	Fe	Cu	Mn	Mg	Cr	Zn	Ti	Al
Contents (%)	0.668	0.545	0.233	0.106	1.098	0.107	0.136	0.029	Bal.

Table 2 Main chemical composition of AZ31B magnesium alloy (mass fraction %)

Elements	Al	Zn	Mn	Si	Fe	Cu	Ni	Mg
Contents (%)	2.96	0.52	0.31	0.16	0.003	0.006	0.001	Bal.

Table 3 Main chemical composition of H13 steel

Elements	C	Si	Mn	P	S	Cr	Mo	V
Contents (%)	0.4	0.973	0.37	0.016	0.019	4.98	1.25	1.01

2.3 Cross-section observations

After the FSW experiment, the standard metallographic preparation procedure was used to prepare weld cross section samples with different parameters, and the sampling position was shown in Fig. 3. Due to the unique design of the pin tool, the initial welding material is insufficient, and the non-conservation area of volume is avoided when selecting the sample position. After grinding and polishing, the samples are corroded. According to different corrosion characteristics, different corrosion solutions were prepared. The aluminum alloy side was corroded by Keller reagent prepared with 95mL distilled water +2.5mL nitric acid +1.5mL hydrochloric acid +1mL hydrofluoric acid; The magnesium alloy side is corroded by caustic agent composed of 5g picric acid +5mL acetic acid +10mL distilled water +100mL absolute ethanol solution. Optical microscopy (OM, Axio Vert.A1) and scanning electron microscopy (SEM, TESCAN LYRA3 GM) were used to observe the microstructure and energy dispersive spectroscopy (EDS) analysis to study its microstructure and material flow.

2.4 Mechanical property

The mechanical properties of lap joints were evaluated by tensile shear test. The tensile shear test was carried out on a universal machine with preload of 0.5kN and tensile speed of 1 mm/min. The selected positions and sizes of tensile and shear samples were shown in Fig. 3. Three samples were selected for each plate for measurement and the average value of the maximum force was taken to evaluate the mechanical properties of the joint. Fig. 4 shows the assembly drawing of the tensile sample. A pad is added at both ends of the sample to ensure that the loading force is in the same direction during the

drawing process. After the test, the fracture morphology was observed under scanning electron microscope, and the fracture mechanism was analyzed.

Results And Discussion

3.1 Macroscopic morphology analysis

The surface quality is a standard used to evaluate the weld quality, and the defects of the weld can often be seen from the surface quality. Fig. 5 and 6 respectively show the overall appearance and weld cross section morphology of Al/Mg and Mg/Al lap joints under different parameters. For the convenience of analysis, the left side of the figure is the macro weld, and the right side is the weld cross section morphology under the corresponding parameters.

As can be seen from the Al/Mg lap bonding mode in Fig. 5, the overall formability of the weld deteriorates when the welding speed remains unchanged and the rotational speed increases, as shown in Fig. 5(a-d). When the rotational speed is 1200r/min, the material accumulation at the retreating side of the weld is serious, and when the rotational speed continues to increase to 1500r/min, multiple bulges appear in the weld center, indicating that there are holes in the weld. The reason may be that with the increase of the rotational speed, the heat input increases, and the welded material is in a highly thermoplastic state. Therefore, under the centrifugal action of the pin tool, the material spills out, resulting in insufficient welded joint materials and forming holes.

Fig. 5(e, b, f) shows the macro weld diagram with constant rotation speed and increased welding speed. It can be found that when the welding speed increases to 60mm/min, there is an obvious tunnel defect in the center of the weld. This is because the pin stays too short at a certain moment in the weld, resulting in insufficient heat input and poor material fluidity. Therefore, the holes formed by the outflow of materials at the previous time cannot be timely filled by the materials at the later time, thus forming tunnel defects[17].

In order to further analyze the forming quality of the weld, the cross section of the weld is analyzed. As shown in Fig. 5(a)-(d), when the welding speed is constant(40mm/min), the tunnel defects tend to increase first and then decrease with the increase of the welding speed, and the material flow trend line near the back side of the weld center moves upward (As shown by the blue dashed line in the figure). Fig. 5(a), (b) and (c) show the increasing trend of the tunnel defect, while Fig. 5(c) and (d) show the tendency of the tunnel to become smaller.

A preliminary analysis of the reasons for the phenomenon of tunnel defects enlargement in Fig. 5 (a-c) shows that with the increase of rotational speed, the effect of underpressure on shoulder decreases[19]. The material in the shoulder area can fill the interspace in the waist area of the needle under the induction of downward pressure, but due to the decrease of downward force, the gap cannot be filled, resulting in holes. With the increase of rotational speed, in the direction of the thickness under the shoulder, less

material is induced to flow downward by the force of the shoulder[12], and the deformed material is more likely to overflow the weld joint in the form of flash[20], thus developing from small holes to tunnel defects.

As can be seen from Fig. 5(a-d), the amount of metal from the lower layer into the upper layer increases with the increase of rotational speed, which is the dominant factor for the reduction of tunnel defects in Fig. 5(a-d). Due to the shoulder design at the top of the needle, the contact area between the SNT and the material is increased, so the heat input of the material in the area around the SNT is improved, and the flow speed is relatively improved.

With the increase of rotational speed, the materials in three areas of the shoulder, the waist of the needle and the SNT all reach the plastic flow state. Due to the special design of the pin, the velocity of the material in the direction of the thickness of the needle below the shoulder varies, showing that the velocity of the shoulder is greater than that of the SNT than that of the waist of the needle. Therefore, at a certain moment, the temporary cavity formed on the advancing side (AS) is preferentially filled by materials near the shoulder region and the SNT region. The higher the rotational speed, the more materials are backfilled to the advancing side and accumulated at the hole of the retreating side, thus filling a part of the tunnel defects and making them smaller. It can be seen from Fig. 5(e), (b) and (f) that the tunnel defects increase with the increase of welding speed, which may be because the heat input decreases with the increase of welding speed and the material fluidity is weak. Moreover, due to the design of the SNT, the temporary hole formed on the advancing side is too large, which promotes the formation of tunnel defects.

Fig. 6 shows the weld formed by Mg/Al lap connection. When the welding speed is unchanged and the rotational speed is increased as shown in Fig. 6(a-d), the semicircular indentation on the weld surface becomes disordered as shown in Fig. 6(d), which may be caused by machine instability caused by defects inside the weld. When the rotating speed is constant increases welding speed is shown in Fig.6 (e, d, f), weld quality decreased obviously, by the indentation of unstable tunnel defects into the center of weld material overflow. This is due to the increase of welding speed, welding heat input is low, resulting in insufficient material fluidity. Besides, the materials on the advancing side flow to the retreating side under the action of the needle, but the retreating side materials fail to go around the back of the needle to fill the defects on the advancing side due to the higher temperature of the advancing side than that of the retreating side. Consequently, a lot of materials accumulate on the retreating side, which is represented by a large number of flashes and accumulation on the retreating side of the weld surface under the action of the shoulder.

The right side of Fig. 6 (a-d) also shows the cross section of the weld with constant welding speed and increased rotation speed.

It can be seen that with the increase of rotational speed, the possible cause of tunnel defects is the same as the Al/Mg lap mode: the increase of rotational speed weakened the effect of the pressure under the

shoulder[19], making the interspace below the waist area of the stirring needle unable to be filled, thus forming hole defects. Fig 6(a) shows the welds obtained under the process parameters of 700r/min and 40mm/min. Although a certain degree of metallurgical reaction was generated at the lap interface, there were obvious cracks. Moreover, the crack runs through the whole lap interface which results in failure connection of the joint.

As shown in Fig. 6(e), (d) and (f), when the speed is unchanged (1500r/min) and the welding speed increases, the weld develops from no defect to obvious hole defect, and the defect becomes larger as the welding speed increases. This is because the welding speed increases, resulting in reducing overall heat input and the fluidity of the material. When the materials on the advancing side flow to the retreating side under the action of the pin tool, and the materials on the retreating side behind the needle flow to the advancing side, due to the fast travel speed of the pin tool, the materials on the advancing and retreating side are stuck on both sides, which leads to the lack of material filling at the center of the weld, and the holes develop into tunnel defects.

Comparing Al/Mg and Mg/Al lap modes, as shown in Fig.5(b-d) and Fig. 6, under the same welding parameters, the internal quality of weld obtained by Mg/Al lap mode is generally good, and only small hole defects appear under the parameter of high speed, while Al/Mg joints are mostly tunnel defects. This is because aluminum has more slip systems than magnesium, so aluminum has higher deformation capacity than magnesium under the same heat input[9]. When the aluminum plate is located at the lower side, due to good deformation ability, the bottom metal fluidity is higher than the lap mode of the magnesium plate located at the lower side, so the heat production at the bottom is higher, which makes up for the shortcoming of low waist heat production, forming good quality weld joints.

3.2 Microscopic morphology analysis of lap joint

3.2.1 Microstructures

By observing Fig. 7, it can be found that the mixing conditions at the lap interface at the bottom of the weld core area obtained by the two lap modes are different. As shown in Fig. 7(a),in the Al/Mg lapping mode, the interstitial layer grows perpendicular to the interface in the fusion zone, indicating insufficient mixing[5], while the Mg/Al lapping joint shown in Fig. 7(b) shows obvious onion ring structure, indicating good mixig at the interface.

According to the EDS line scanning diagram in Fig.8 and 9, the mixing of magnesium and aluminum can be clearly seen. The line scanning path is always from the bottom to the top of the weld joint. Regardless of the Al/Mg or Mg/Al lap mode, the overall content of magnesium in the interfacial mixing zone is always greater than that of aluminum. That is to say, the mixing zone at the interface is a magnesium-rich zone, and the mixing zone is a region where intermetallic compounds are generated in large quantities. According to the XRD test results in Fig. 10 and 11, it can be seen that the intermetallic

compounds are $Al_{12}Mg_{17}$ (γ) and Al_3Mg_2 (β). Therefore, combined with the results of EDS line scanning, it can be inferred that the generation condition of $Al_{12}Mg_{17}$ in the mixed zone is better than that of Al_3Mg_2 in the two lap bonding modes. The difference is that the mixing degree of aluminum and magnesium is not consistent in the thickness direction of the interfacial mixing zone of the weld obtained by the two lap joints. As shown in Fig.8,the magnesium content in the upper layer of the mixing zone of Al/Mg lap joint is less than that in the lower layer of the mixing zone, indicating that the mixing degree of aluminum and magnesium in the upper part of the mixing zone of Al/Mg lap joint is not as good as that at the bottom, and the mixing is not sufficient, which is consistent with Ji, S et al.'s[13] research results. This also echoes the previous conclusion that the interface in Fig.7 (a) is not sufficiently mixed. The line scan result of Mg/Al lap joint shown in Fig.9 shows that although the content of Al and Mg fluctuates in the thickness direction, it is basically stable, which indicates that the mixing degree of aluminum and magnesium in the mixing layer under the Mg/Al lap mode is good, which also verifies the layered structure of the mixing zone of Mg/Al joint.

In addition, as shown in Fig. 8(b-d), when the welding speed is unchanged and the rotational speed is increased, it is observed that under the action of pin tool, more magnesium alloy of the lower plate flows upward. When the rotational speed is increased to 1000r/min, the content of aluminum alloy of the upper plate in the middle of the mixing zone suddenly decreases, which is related to the decrease of the downward force of shoulder after increasing the rotational speed of the pin tool. When the speed increases to a certain extent (1200r/min), the aluminum and magnesium content in the mixing zone gradually tends to be stable, that is to say, the aluminum and magnesium mixing situation in the mixing zone is good, and the distribution is uniform. Similarly, at the rotational speed of 1500r/min in Fig.9(c), magnesium alloy in the upper plate shows a phenomenon of high content in the upper layer and low content in the lower layer in the mixing zone, which is also the reason for the reduction of the axial shoulder force. This phenomenon is consistent with Boccarusso, Let al.'s[19] research.

Fig. 10(a) and (b) show the XRD test results of Al/Mg weld cross section at 800r/min-40mm/min and 1200r/min-40mm/min. It can be seen that the number of intermetallic compounds increases with the increase of speed (from 800r/min to 1200r/min). Due to the existence of welding defects, the detection results are bound to be affected to some extent. However, it can be seen from Fig.5(a-d) that with the increase of rotational speed, the tunnel defects show an increasing trend, and the XRD test results show that the number of IMCs still increases, which further proves the conclusion that the heat input increases and intermetallic compounds increase. It is found that when IMCs increases, the peak of Al_3Mg_2 is stronger than that of $Al_{12}Mg_{17}$ at 800r/min-40mm/min welding parameters, and with the increase of heat input, the increase of IMCs-$Al_{12}Mg_{17}$ is greater than that of Al_3Mg_2.It is speculated that this is because the design of the SNT increases the fluidity of magnesium at the stirring needle end and makes it contact with more aluminum (as can be seen from the EDS line scan results of the two joints), thus increasing the conditions for the formation of $Al_{12}Mg_{17}$.

Fig.11(a) and (b) show the XRD test results of the cross-section of Mg/Al welds at 1000r/min-40mm/min and 1000r/min-60mm/min. Similar to the test results of Al/Mg joints above, with the increase of rotational speed, the heat input increases, leading to the increase of intermetallic compounds. Similarly, with the increase of heat input, the peak intensity of $Al_{12}Mg_{17}$ increases, indicating that the content of $Al_{12}Mg_{17}$ is always higher than that of Al_3Mg_2 when the heat input is higher in either type of lap bonding. In Mg/Al lap welding of AZ31B and Al 6061,Beygi, R et al.[21] proposed that Al + Al_3Mg_2 eutectic has higher Al concentration, higher melting temperature and higher viscosity than $Al_{12}Mg_{17}$ intermetallic compound, thus limiting the flow and mixing of the material in the weld. This also explains the phenomenon that the content of $Al_{12}Mg_{17}$ is higher than that of Al_3Mg_2 in the mixing zone in this paper.

Fig.12 shows the microscopic diagram of the advancing side and retreating side of the weld joints obtained under the two lap modes. It is found that a continuous layered material appears on the side where the mixing zone contacts aluminum (the area marked by the red arrow in the figure), and its composition is found by EDS analysis to be Al+Al_3Mg_2 eutectic, as shown in Fig. 13(a). Zhai, M et al.[22] and R. Beygi et al.[21] also found similar morphology in lap welding of aluminum and magnesium, and found that this layered material was also intermetallic compound Al_3Mg_2 layer through testing and analysis. Moreover, EDS test on the black area showed that the black area contained more magnesium, mainly Mg+$Al_{12}Mg_{17}$, as shown in Fig.13(b). This is also consistent with the conclusion that Al_3Mg_2 is formed near aluminum and $Al_{12}Mg_{17}$ is formed near magnesium. The thickness of the continuous IMCs layer is marked in Fig. 12. It is found that the thickness of the IMCs layer in contact with the black region (the Mg+$Al_{12}Mg_{17}$ region) is smaller, while the IMCs layer generated in the position without the black region is thicker. This is because the black region is magnesium and its eutectic structure, and there is no composition gradient at the contact interface with the IMCs layer, which limits the diffusion of aluminum and magnesium, so the growth of the IMCs layer is limited [21].However, there is no such eutectic structure in the brown area, so the kinetic energy of the element increases with the increase of temperature in the welding process, which gives favorable conditions for the diffusion of aluminum and magnesium, so the IMCs layer thickens.

3.2.2 Hook features

Fig.14 and 15 show the micro morphology of the forward side and backward side of the weld obtained under the two lap modes of Al/Mg and Mg/Al, respectively. It can be seen that hook defects inevitably occur no matter what kind of lap bonding method. In fact, hook is a kind of inherent feature appearing in FSW weld joints. It is characterized as a crack-like unbonded interface that deformed from the original surfaces on both AS and RS[23].The formation of hook can be interpreted as the following discussions.

In friction stir lap welding, the lap interface is perpendicular to the pin tool. When the stir needle penetrates the lap interface in the welding core area, the interface oxide layer in the SZ area is destroyed. However, the interface outside the stir needle cannot be stirred and broken sufficiently, so the position of

this interface will shift with the flow of nearby materials. With the rotation of the pin tool, the materials in the SZ zone will flow downward and gather at the terminal of the stirring needle. The accumulated materials will force the materials in the thermo-mechanical affected zone to flow upward, so as to push the lap boundary to bend upward. Generally, the bending interface on the retreating side is subjected to the backward shear force and bends toward the direction of stirring needle rotation, while the bending interface on the advancing side remains vertical, and finally a hook and cold lap are formed on the advancing side and the retreating side, respectively. The hook shape affects the effective plate thickness (EST) and effective lap width (ELW),which are often used to quantitatively describe the lap quality[13].EST is the minimum distance from the highest point of the hook tip or cold lap joint to the upper surface of the upper plate. ELW is the width of the bond region from AS to RS[24].

It can be found from Fig. 14 that under Al/Mg lap mode, the forward side of the weld presents cold lap defects, and the backward side presents hook defects. Tan, S et al.[14] reported the microstructure characteristics of the lapping of 6061 aluminum alloy and NZ30K magnesium alloy. It can be seen from the cross-sectional diagram in the paper that the cold lapping and hook defects formed on the advancing and retreating sides are similar to those in Fig. 14 (a). While in Fig. 14 (b) and (c), the advancing side is cold lapping, and the retreating side lapping interface does not move upward, but moves downward, forcing the upper plate material into the lower plate to form a defect. Although not like the normal hook defect, but extend into the lower plate of the end is also sharp. This is because the design of the SNT gives the flowing material an upward oblique thrust, changing the flow path of the material, as shown by the blue arrow in Fig. 16. Considering that the fluidity of the aluminum alloy on the upper plate is better than that of the magnesium alloy on the lower plate, the upper plate material continues to flow into the lower plate, and because of the extrusion action of the surrounding unplasticized material, a unique retreating side defect shape is formed.

The other Mg/Al lap mode is shown in Fig. 15. Both the advancing side and the retreating side show hook defects, and with the increase of welding speed, the effective plate thickness (EST) of the advancing side and the retreating side increases significantly, that is, the hook height decreases (The height from the highest point of the hook to the bottom of the mixing layer is shown in the figure). At the same time, the width of the hook in the horizontal direction is reduced, and the overall appearance is steeper. First of all, due to the increase of welding speed, the low heat input reduces the fluidity of the material, which leads to the reduction of the induction effect of stirring on the material in the weld core area, so the upward extension distance of the hook becomes shorter. This is the same as Song, Y et al.'s[23] research result. Similarly, at a low welding speed, the material has large heat input and strong fluidity, which makes the material on the AS side and RS side easy to flow upward, so the hook extends a large distance upward. On the other hand, due to the fixed speed, it means that the downward pressure on the shoulder is the same, and the downward pressure on the lap interface is the same. Due to the different welding speeds, the greater the welding speed, the worse the material fluidity will be. Therefore, the materials in the SZ area gather and accumulate at the bottom, pushing the lap boundary to both sides, resulting in the steep hook defect.

However, with the increase of the rotational speed, the EST of the advancing and retreating side does not change obviously, and the EST of the advancing side slightly increases, while the EST of the retreating side slightly decreases. In the horizontal direction, the width of the advancing and retreating hooks increases, because with the increase of the speed, the heat input of the material increases, the heat affected zone expands, the fluidity of the external material of the pin tool increases, and it is more likely to be induced by the pin tool to move closer to the welding core area, which is shown as the increase of the hook width in morphology.

By comparing Fig. 14 and Fig. 15, it can be clearly seen that the lap interface mixing of Mg/Al lap mode is better than that of Al/Mg lap mode. This is because of the good flow performance of aluminum alloy. When the aluminum plate is placed on the lower plate, although the heat input is lower than that of the upper plate, its good fluidity makes up for this defect, so that the two materials mix well at the lap interface and form an onion ring with lamellar structure[25]. Ji, S et al.[13] also studied the weld hook defects obtained by welding AZ31B magnesium alloy and 6061 aluminum alloy in Mg/Al lap mode, and found that the hook defects obtained by conventional pin tool are prone to the hook defects that bend upward nearly 90 degrees. However, such hook defects did not appear in this paper, instead, a smooth hook defect was found. This is because the pin tool in this paper has increased the design of the large diameter SNT at the end. As the shoulder diameter of the end part is large, the starting point of the hook defect is far away from the weld center, which also increases the width of the hook defect. On the other hand, the material flow track shown by the blue arrow in Fig.16 has a certain inhibitory effect on the generation of hook defects[26]. Under the action of both, the unique hook defect shown in this paper is formed.

3.3 Fracture morphology and mechanical properties analysis

Fig.17 and 18 show the change of failure load of friction stir welding joints welded at different rotation and welding speeds. As shown in Fig. 17, Al/Mg failure load variation diagram, when the welding speed remains unchanged and the rotation speed increases, the failure load decreases at the rotation speed of 1200r/min and 1500r/min, while the load increases at the rotation speed of 1000r/min. Combined with the macro analysis of 3.1 and the hook defect analysis of 3.3.3, it is concluded that the advancing side of the weld is cold lash defect under the process parameters of 1000r/min and 40mm/min, while the retreating side has no hook defect due to the SNT design, and the mechanical interlocking degree is high, which is conducive to improving the failure load[27, 28]. When the rotation speed is unchanged and the welding speed is increased, it can be seen that when the welding speed is increased to 60mm/min, the load is greatly reduced and the joint performance deteriorates sharply. When the welding speed is 20mm/min and 40mm/min, the joint failure load is higher, but the failure load of 20mm/min joint is lower than 40mm/min, which is related to the generation and distribution of the joint IMCs. The reduction of welding speed greatly increases the heat input of the joint. As can be seen from Fig. 7 (a) and Fig. 12, most intermetallic compounds are generated at the advancing side and retreating side of the interface and at the bottom of the welding core area, which is prone to stress concentration and crack initiation

and development. The generation of IMCs hard phase further aggravates the deterioration of the joint properties. By comparing Fig. 17 and 18, it can be found that the failure load of Al/Mg lap joint is better than that of Mg/Al lap joint on the whole. It can be seen from the figure that this is because the fracture of Mg/Al lap joint is completely along the edge of the interface mixing layer, which is weak bonding. However, because no obvious mixed layer was formed in Al/Mg lap joint, the fracture occurred along the weld core area, which was speculated to be caused by internal micro-cracks. Therefore, Mg/Al lap joints have lower failure loads at break than Al/Mg lap joints. It can be seen from Fig. 15 (c) that the hook defect is round and the thickness of the effective lap board is the largest, so this is also the reason for the maximum failure load. Because the tip of the hook defect is the most important factor in the development of the inducement crack.

Fig. 20(a)(b) shows the SEM morphology of the aluminum side under the Al/Mg lap mode, and Fig. 21(c)(d) shows the mg side of the fracture. It can be seen that both sides of the fracture have the characteristics of cleavage and ductile fracture, respectively. However, the fracture on the magnesium side is generally flat, while the fracture on the aluminum side is very uneven, and the dimple size on the magnesium side is smaller than that on the aluminum side. Fig. 20 (a) and (c) fractures show cleavage patterns, which are the main characteristics of brittle fractures and result from the presence of IMCs layers at the interface. This morphology is very similar to the results of the Beygi, R's[21] study, in this case, the joint shows weak bonding and the fracture is more likely to propagate through the thick and continuous IMCs layer at the joint interface. According to Chang, W's[6] research, the intermetallic phase of Al3Mg2 and $Al_{12}Mg_{17}$ is the reason for the low ductility of the friction stir welding joint of al 6061/AZ31B dissimilar alloy. The fracture morphology in Fig. 20 (b) and (d) is similar to the results of Ji, S's[13] study. A large number of dimples of very small size and depth can be observed in the figure, showing a ductile fracture pattern. In this case, the bonding line remains intact and the fracture expands in Mg by shear plastic deformation[21].

The fracture morphology of Fig.21 (a-c) was taken from the magnesium side, and (d-f) from the aluminum side. The morphology of Fig.21 (a) and (d) was similar to the results of Ji, S's[13] study, showing ridges formed during the movement of the pin tool. Figures (b) and (f) mainly show the morphology of intercrystal and cleavage. There are small dimples between the fractures. Dimples are characteristic of ductile fracture of Mg (Al) in eutectic mixture. As mentioned earlier in the tissue analysis, the eutectic structure impedes the growth of continuous IMC layers resulting from solid state diffusion. Therefore, the fracture does not occur through the continuous IMC layer, but propagates through the eutectic zone. Eutectic region includes intermetallic phase and eutectic Mg (Al), while Mg (Al) is relatively soft phase. In the loading process of the weld joint, the small crack in the weld and the sharp hook defect will induce the crack and defect expansion, resulting in fracture. Due to the presence of soft phase Mg(Al), the crack propagation is hindered to a certain extent, and the crack propagation is limited, which is manifested as small dimples in some areas on the fracture, and therefore the joint strength is increased[21].

Conclusion

Lap welding of Al-Mg dissimilar alloy was successfully achieved by using the new pin tool. Formability, microstructure defects and mechanical properties of Al-Mg dissimilar lap joint under the SNT were studied. The main research results are as follows:

1. Due to the design of the SNT, the flow direction of the material in the heat affected zone is directly changed, and the shape of the hook defect at the interface of the lap Mg/Al joint is changed, which increases the EST and effectively improves the mechanical properties of the lap joint.

2. No hook defect appeared on the back side of Al/Mg lap joint obtained under the process parameters of 1000r/min and 40mm/min, and the maximum failure load reached 4.8KN, indicating that SNT coordinated the flow of the upper and lower plates.

3. Because of the design of SNT, the mixing degree of Al-Mg dissimilar materials in the direction of plate thickness is improved.

Declarations

Available of data and material All data produced or analyzed during this study are included in this published article.

Competing Interests The authors declare no competing interests.

Author Contributions All authors contributed to the study conception and design. The first draft of the manuscript was written by Tianfan Jiang and all authors commented on previous versions of the manuscript.

Tianfan Jiang: investigation, analysis, writing——original draft preparation. Jinpeng Hu: Material preparation, data collection. Yifu Shen: investigation, reviewing and editing, supervision. Tao Sun: data collection, reviewing and editing. Ruiyang Ni: reviewing and editing. Fujun Cao: reviewing and editing. Tao Yu: reviewing and editing. Guangming Zhou: reviewing and editing.

References

1. T. Sun, Y. Shen, F. Cao, Y. Yan, R. Ni, J. Jin, (2022) Forming mechanisms and mechanical property of AZ31B/2024-T4 friction stir welded T-joints. Journal of Adhesion Science and Technology: The International Journal of Theoredtical and Basic Aspects of Adhesion Science and Its Applications in All Areas of Technology (9/12):36.
2. S. Tao, W. Siyu, Y. Shen, J. Jiayi, L. Jiazhu, Q. Tianxiang, M. Catauro, (2020) Effect of Traverse Speed on the Defect Characteristic, Microstructure, and Mechanical Property of Friction Stir Welded T-Joints of Dissimilar Mg/Al Alloy. Advances in Materials Science and Engineering 2020:1-15.

3. T. Sun, Y. Shen, R. Ni, W. Hou, Y. Yan, F. Cao, (2022) Influences of Process Parameters on Morphology and Mechanical Properties of FSW-T-Joint of 2024/5083 Al Alloy Sheets. Arabian Journal for Science and Engineering.
4. S. Wu, T. Sun, Y. Shen, Y. Yan, R. Ni, W. Liu, (2021) Conventional and swing friction stir spot welding of aluminum alloy to magnesium alloy. The International Journal of Advanced Manufacturing Technology 116(7-8):2401-2412.
5. A. Bandi, S.R. Bakshi, (2020) Effect of Pin Length and Rotation Speed on the Microstructure and Mechanical Properties of Friction Stir Welded Lap Joints of AZ31B-H24 Mg Alloy and AA6061-T6 Al Alloy. Metallurgical and Materials Transactions A 51(12):6269-6282.
6. W.S. Chang, S.R. Rajesh, C.K. Chun, H.J. Kim, (2011) Microstructure and Mechanical Properties of Hybrid Laser-Friction Stir Welding between AA6061-T6 Al Alloy and AZ31 Mg Alloy. JOURNAL OF MATERIALS SCIENCE & TECHNOLOGY 27(3):199-204.
7. Z. Shen, S. Chen, L. Cui, D. Li, X. Liu, W. Hou, H. Chen, Z. Sun, W.Y. Li, (2022) Local microstructure evolution and mechanical performance of friction stir additive manufactured 2195 Al-Li alloy. MATERIALS CHARACTERIZATION 186:111818.
8. W.T. Hou, Y.Q. Ding, G.Q. Huang, N. Huda, L.H.A. Shah, Z.Y. Piao, Y.F. Shen, Z.K. Shen, A. Gerlich, (2022) The role of pin eccentricity in friction stir welding of Al-Mg-Si alloy sheets: microstructural evolution and mechanical properties. INTERNATIONAL JOURNAL OF ADVANCED MANUFACTURING TECHNOLOGY 121(11-12):7661-7675.
9. R. Zettler, (2006) Dissimilar Al to Mg alloy friction stir welds. ADVANCED ENGINEERING MATERIALS 8(5):415-421.
10. V. Firouzdor, S.D. Kou, (2010) Formation of Liquid and Intermetallics in Al-to-Mg Friction Stir Welding. METALLURGICAL AND MATERIALS TRANSACTIONS A-PHYSICAL METALLURGY AND MATERIALS SCIENCE 41 A (12):3238-3251.
11. Y.C. Chen, K. Nakata, (2008) Friction stir lap joining aluminum and magnesium alloys. SCRIPTA MATERIALIA 58(6):433-436.
12. J. Mohammadi, Y. Behnamian, A. Mostafaei, H. Izadi, T. Saeid, A.H. Kokabi, A.P. Gerlich, (2015) Friction stir welding joint of dissimilar materials between AZ31B magnesium and 6061 aluminum alloys: Microstructure studies and mechanical characterizations. Materials Characterization 101:189-207.
13. S.D. Ji, Z.W. Li, L.G. Zhang, Z.L. Zhou, P. Chai, (2016) Effect of lap configuration on magnesium to aluminum friction stir lap welding assisted by external stationary shoulder. MATERIALS & DESIGN 103:160-170.
14. S. Tan, F.Y. Zheng, J. Chen, J.Y. Han, Y.J. Wu, L.M. Peng, (2017) Effects of process parameters on microstructure and mechanical properties of friction stir lap linear welded 6061 aluminum alloy to NZ30K magnesium alloy. JOURNAL OF MAGNESIUM AND ALLOYS 5(1):56-63.
15. Z.L. Liu, X.C. Meng, S.D. Ji, Z.W. Li, L. Wang, (2018) Improving tensile properties of Al/Mg joint by smashing intermetallic compounds via ultrasonic-assisted stationary shoulder friction stir welding.

JOURNAL OF MANUFACTURING PROCESSES 31:552-559.

16. X.Q. Lv, C.S. Wu, C.L. Yang, G.K. Padhy, (2018) Weld microstructure and mechanical properties in ultrasonic enhanced friction stir welding of Al alloy to Mg alloy. JOURNAL OF MATERIALS PROCESSING TECHNOLOGY 254:145-157.
17. M.S. Farahani, M. Divandari, (2016) Effect of Zn Interlayer on Microstructure and Mechanical Properties of Dissimilar Al/Mg Weld by FSW. International Journal of Systems Signal Control & Engineering Applications 9(3/4):86-96.
18. B. Zheng, L. Zhao, Q.Q. Lv, G. Wan, D. Cai, S.J. Dong, X.B. Hu, (2020) Effect of Sn interlayer on mechanical properties and microstructure in Al/Mg friction stir lap welding with different rotational speeds. MATERIALS RESEARCH EXPRESS 7(7):076504.
19. L. Boccarusso, A. Astarita, P. Carlone, F. Scherillo, F. Rubino, A. Squillace, (2019) Dissimilar friction stir lap welding of AA 6082-Mg AZ31: Force analysis and microstructure evolution. JOURNAL OF MANUFACTURING PROCESSES 44:376-388.
20. R. Crawford, G.E. Cook, A.M. Strauss, D.A. Hartman, (2006) Modelling of friction stir welding for robotic implementation. International Journal of Modelling. Identification and Control 1(2):101.
21. R. Beygi, H. Pouraliakbar, K. Torabi, B.G. Eisaabadi, V. Fallah, S.K. Kim, R. Shi, L.F.M. da Silva, (2021) The inhibitory effect of stir zone liquefaction and eutectic-phase formation on the growth of gamma/beta intermetallics during dissimilar FSW of Al/Mg alloys. JOURNAL OF MANUFACTURING PROCESSES 70:152-162.
22. M. Zhai, C.S. Wu, L. Shi, (2022) Influence of tool pin length and dissimilar material configuration on friction stir lap welding of Al and Mg alloys. INTERNATIONAL JOURNAL OF ADVANCED MANUFACTURING TECHNOLOGY 122(3-4):1567-1582.
23. Y.B. Song, X.Q. Yang, L. Cui, X.P. Hou, Z.K. Shen, Y. Xu, (2014) Defect features and mechanical properties of friction stir lap welded dissimilar AA2024-AA7075 aluminum alloy sheets. MATERIALS & DESIGN 55:9-18.
24. Z.W. Li, Y.M. Yue, S.D. Ji, P. Chai, Z.L. Zhou, (2016) Joint features and mechanical properties of friction stir lap welded alclad 2024 aluminum alloy assisted by external stationary shoulder. MATERIALS & DESIGN 90:238-247.
25. S.D. Ji, Z.W. Li, (2017) Microstructure and mechanical properties of friction stir lap welded Mg/Al joint assisted by stationary shoulder. METALS AND MATERIALS INTERNATIONAL 23(6):1158-1167.
26. J.L. Liu, Z.L. Hao, Y.M. Xie, X.C. Meng, Y.X. Huang, L. Wan, (2022) Interface stability and fracture mechanism of Al/Steel friction stir lap joints by novel designed tool. JOURNAL OF MATERIALS PROCESSING TECHNOLOGY 300.
27. Mohammadi, J., Behnamian, Y., Mostafaei, A., & Gerlich, A. P. (2015) Tool geometry, rotation and travel speeds effects on the properties of dissimilar magnesium/aluminum friction stir welded lap joints. Materials & Design 75: 95–112.
28. P. Su, A. Gerlich, M. Yamamoto, T.H. North, (2007) Formation and retention of local melted films in AZ91 friction stir spot welds. JOURNAL OF MATERIALS SCIENCE 42(24):9954-9965.

Figures

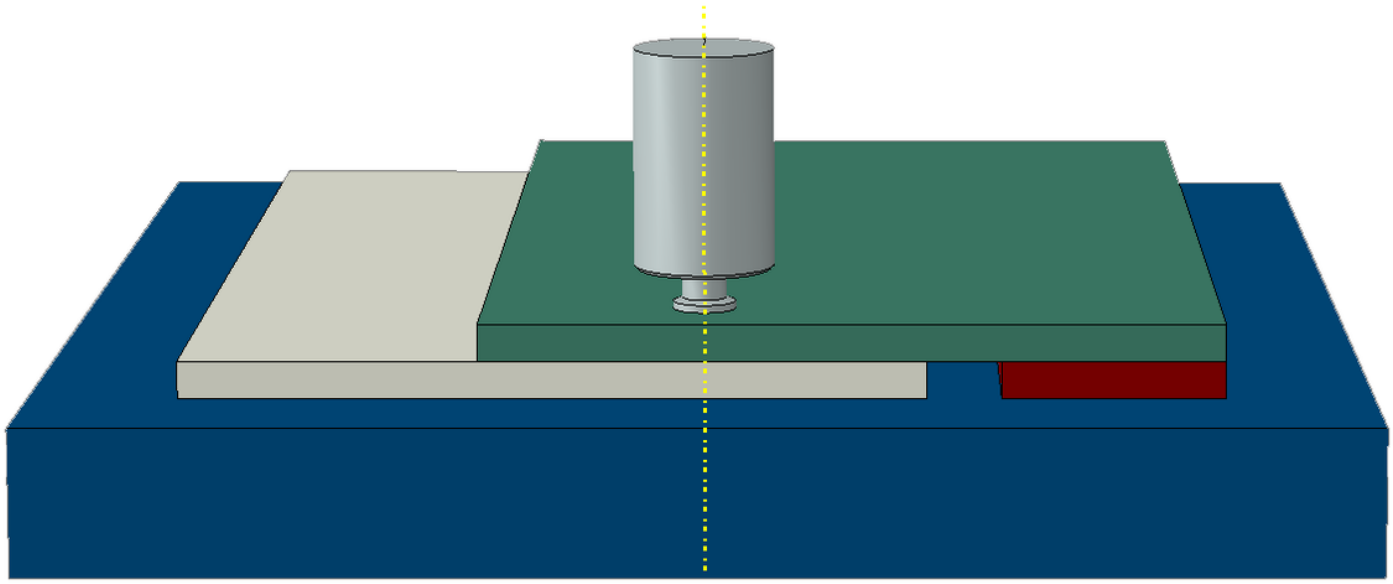

Figure 1

Welding process assembly drawing of FSW

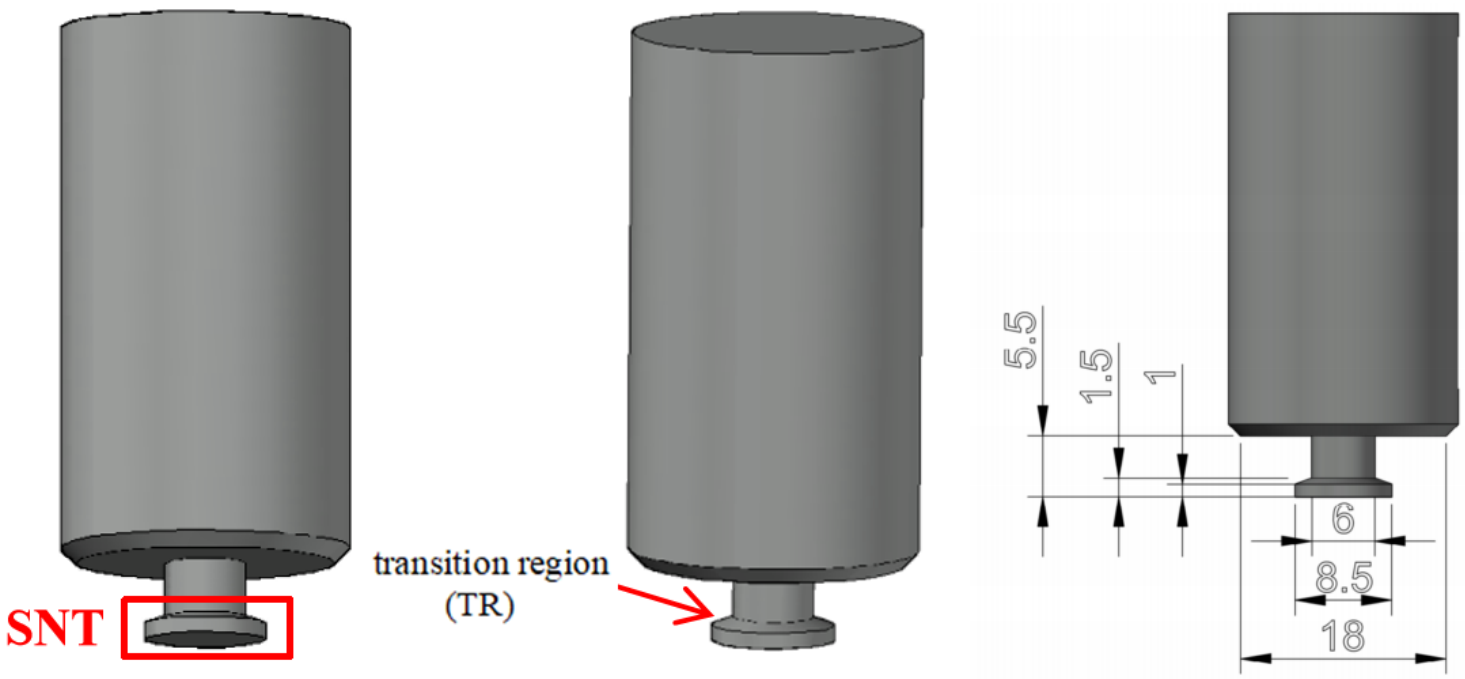

Figure 2

Pin tool space structure diagram

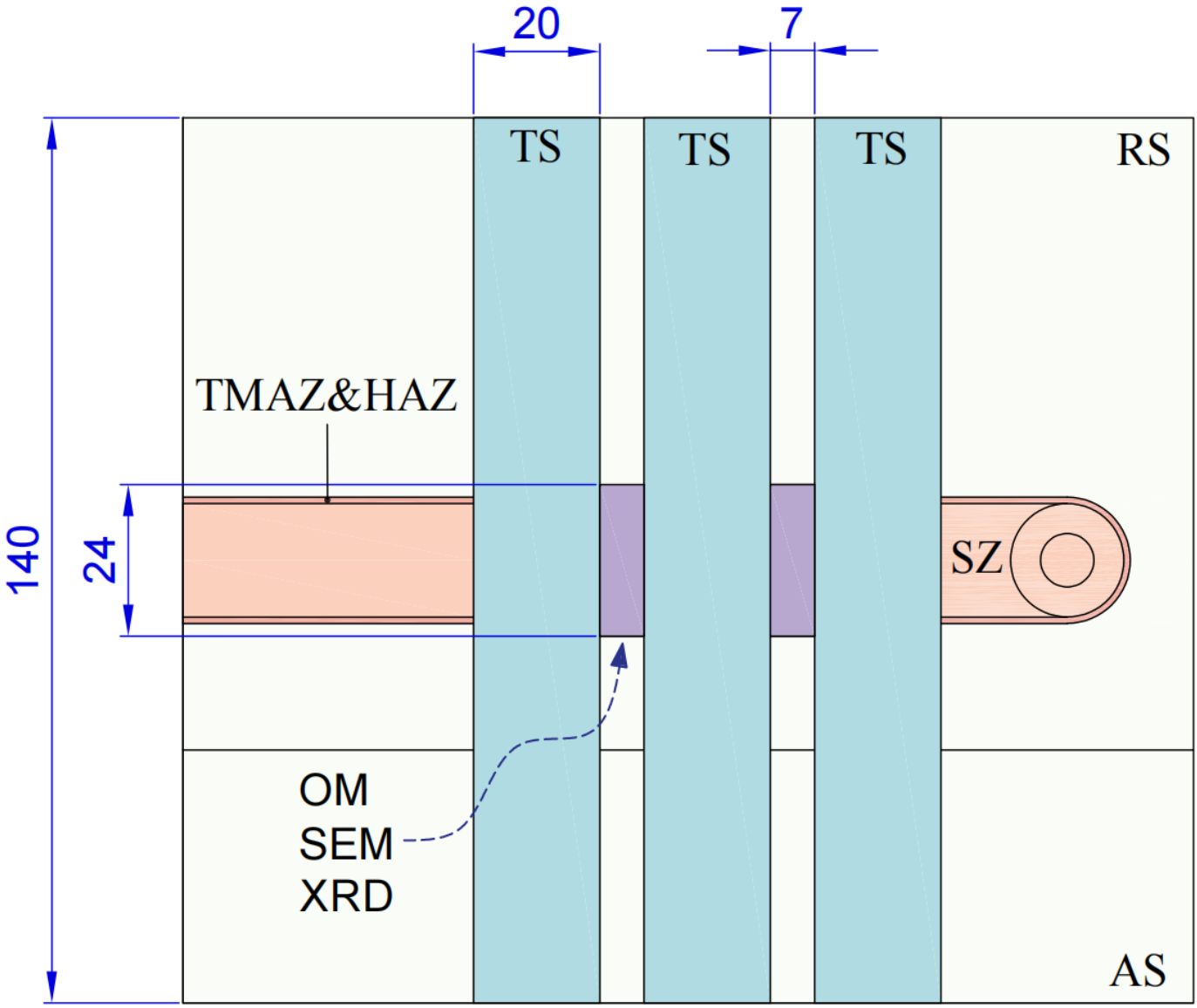

Figure 3

Sampling locations of tensile and metallographic samples

Figure 4

Schematic diagram of tensile performance test

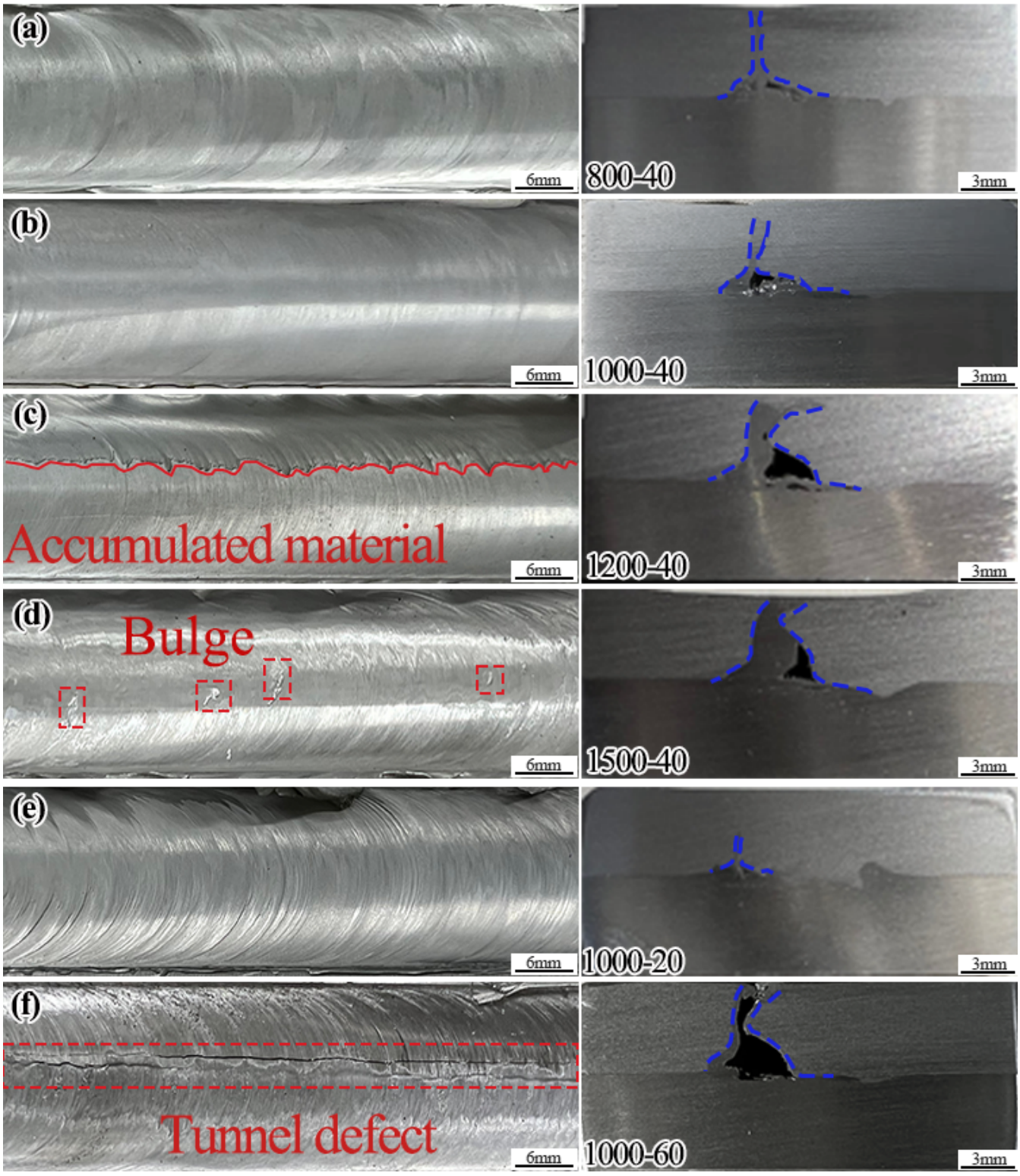

Figure 5

Weld and cross section morphology of Al/Mg lap joints

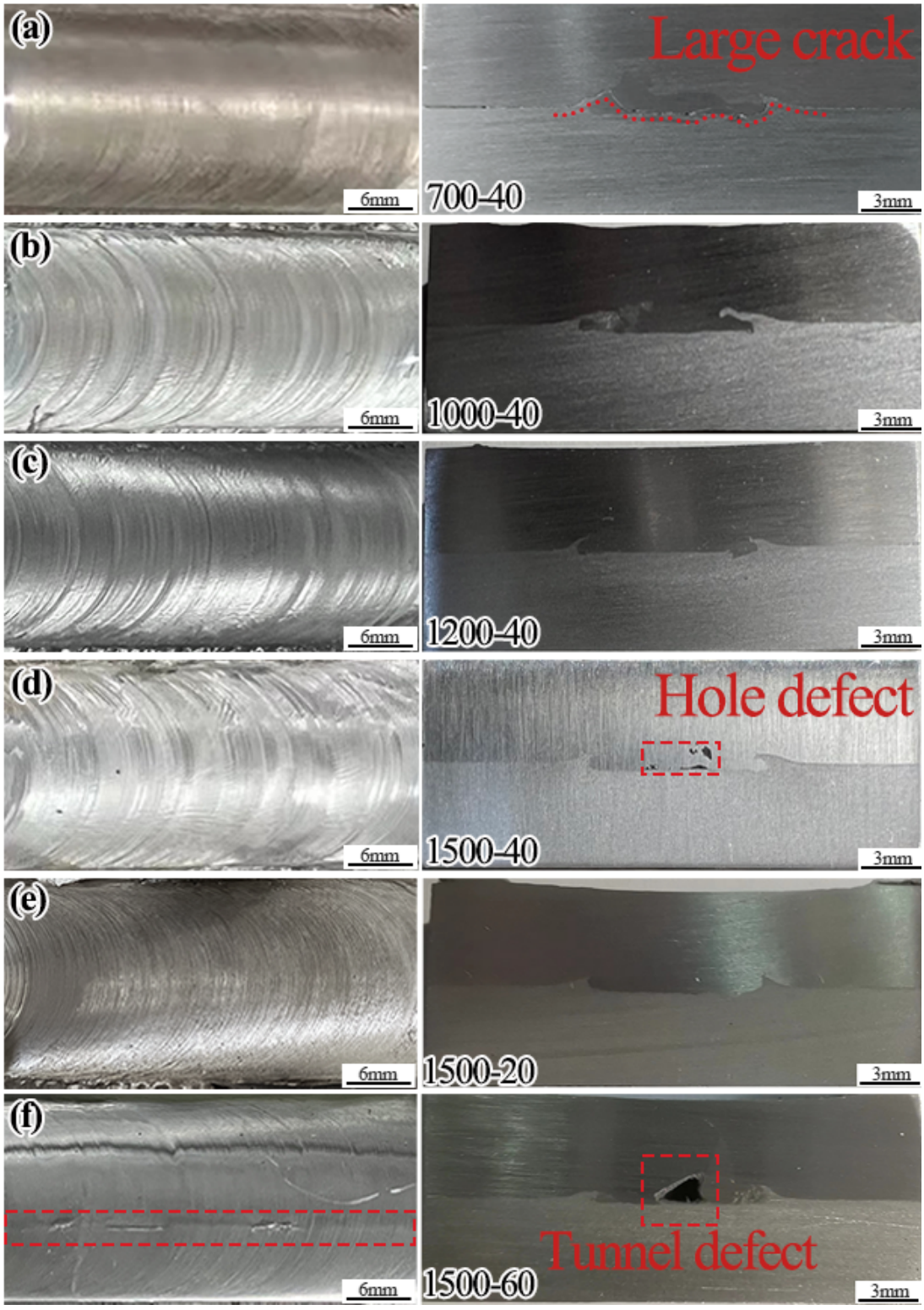

Figure 6

Weld and cross section morphology of Mg/Al lap joints

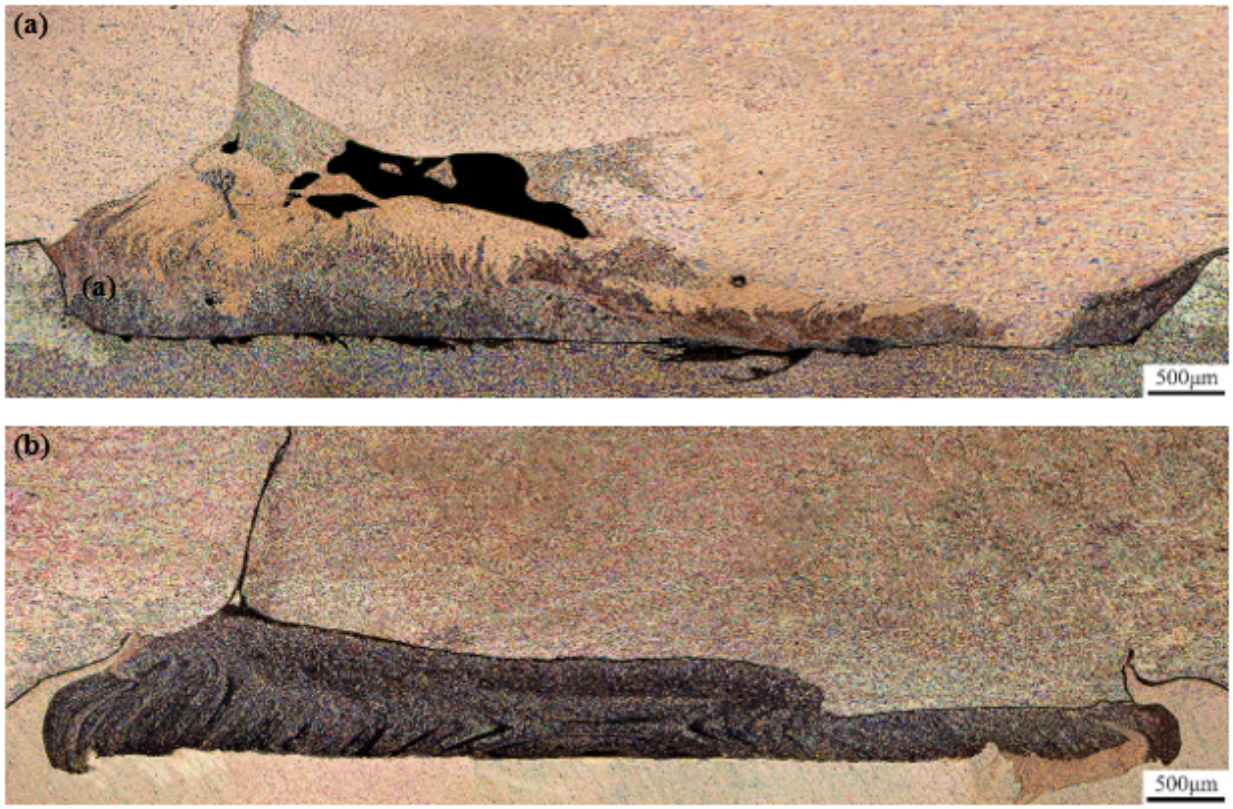

Figure 7

Cross section morphology of mixing zone at lap interface(a)Al/Mg joint(b)Mg/Al joint

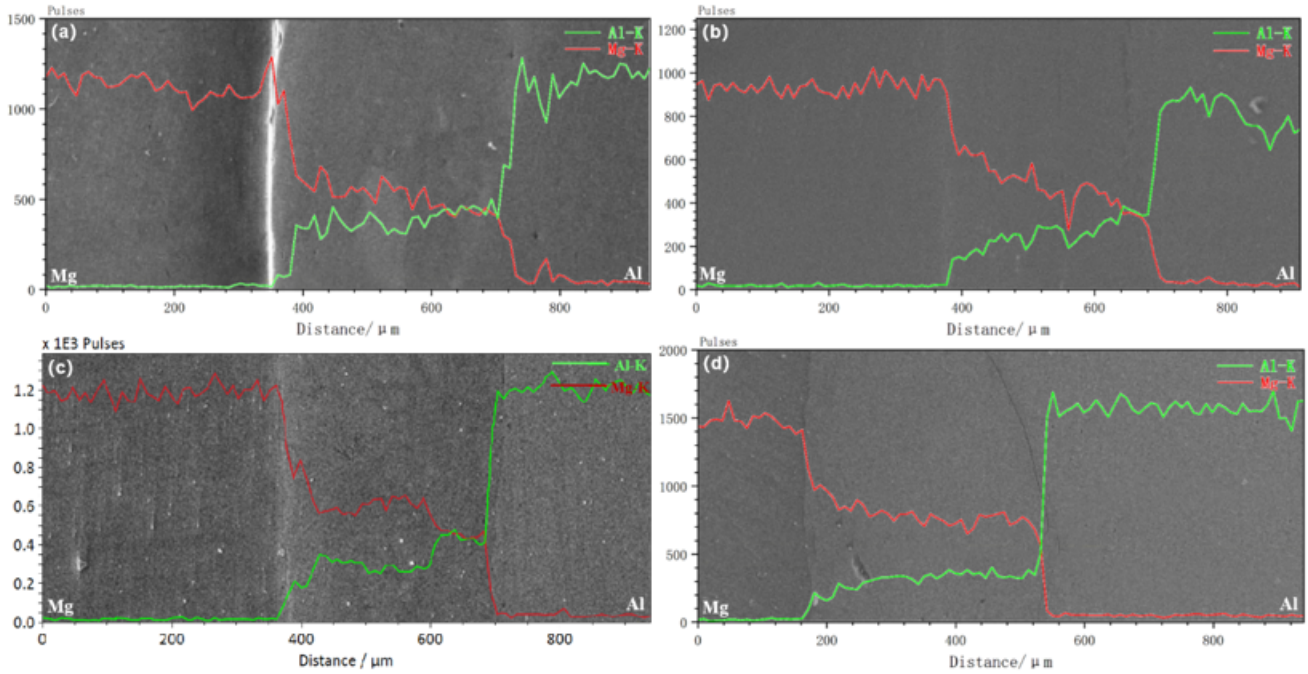

Figure 8

EDS results of the mixing layer at Al/Mg lap interface:(a)1000r/min-20mm/min;

(b)800r/min-40mm/min;(c)1000r/min-40mm/min;(d)1200r/min-40mm/min;

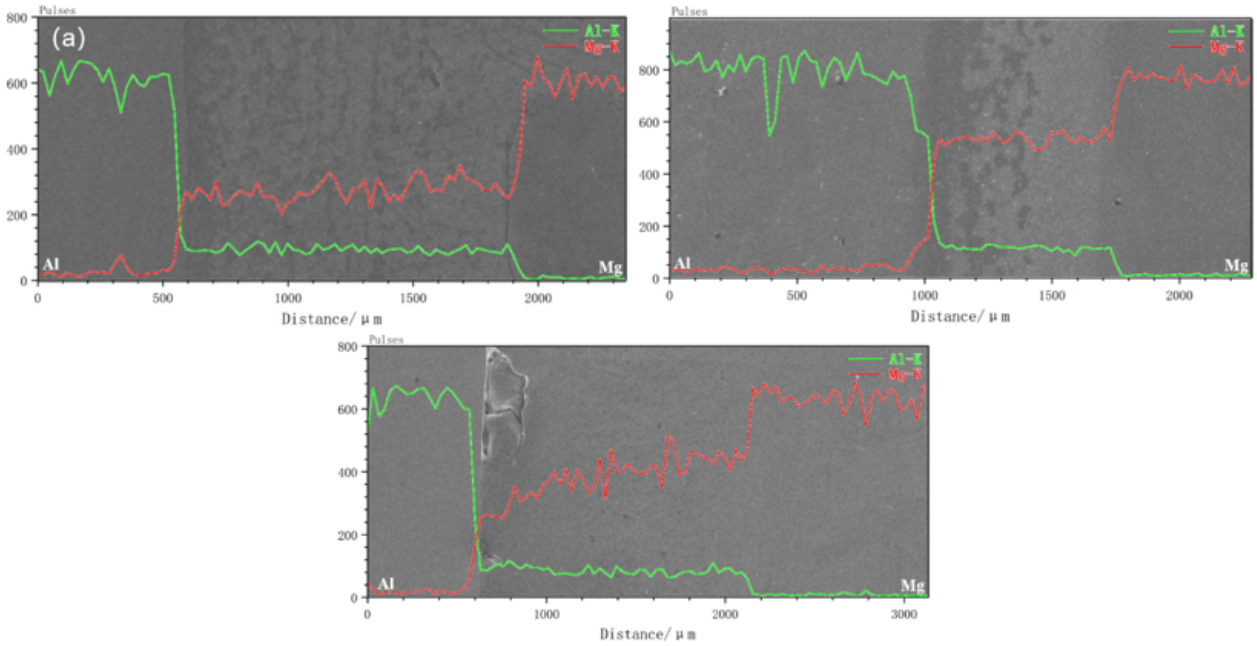

Figure 9

EDS results of the mixing layer at Mg/Al lap interface:(a)1000r/min-40mm/min;

(b)1200r/min-40mm/min;(c)1500r/min-40mm/min;

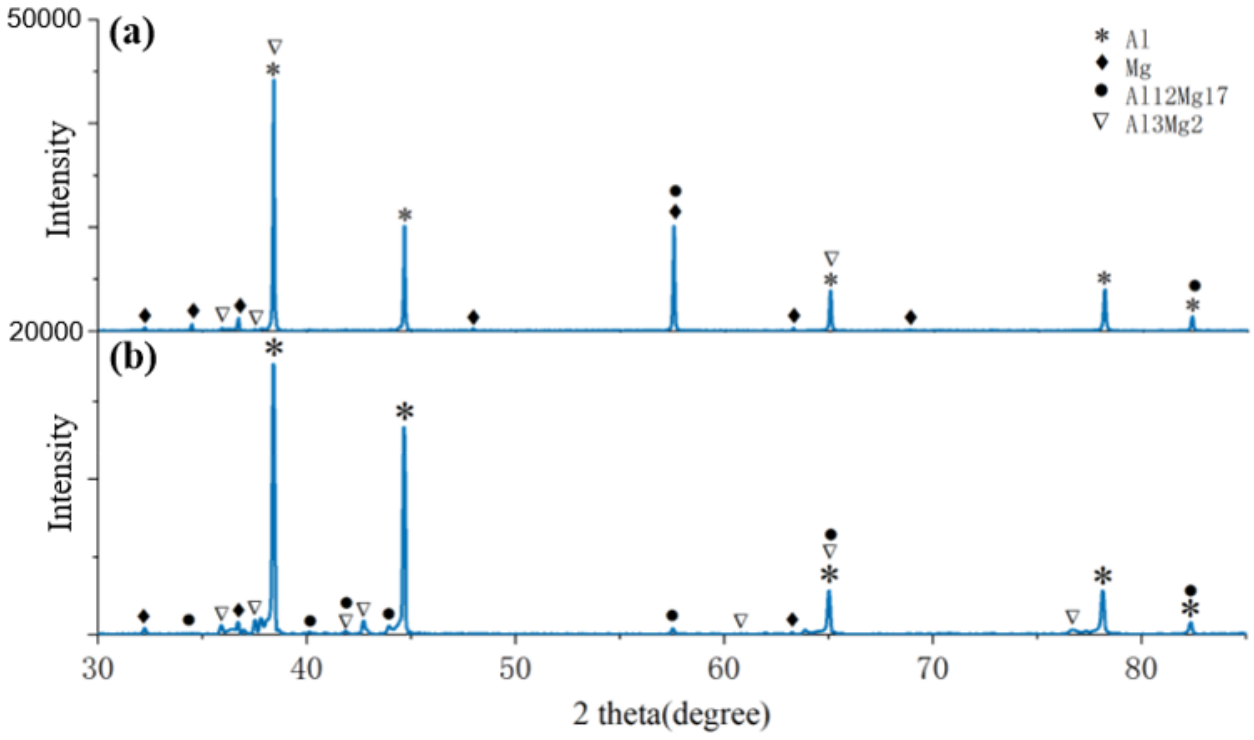

Figure 10

Micro-XRD spectrums from Al/Mg joint cross section:

(a)800r/min-40mm/min;(b)1200r/min-40mm/min

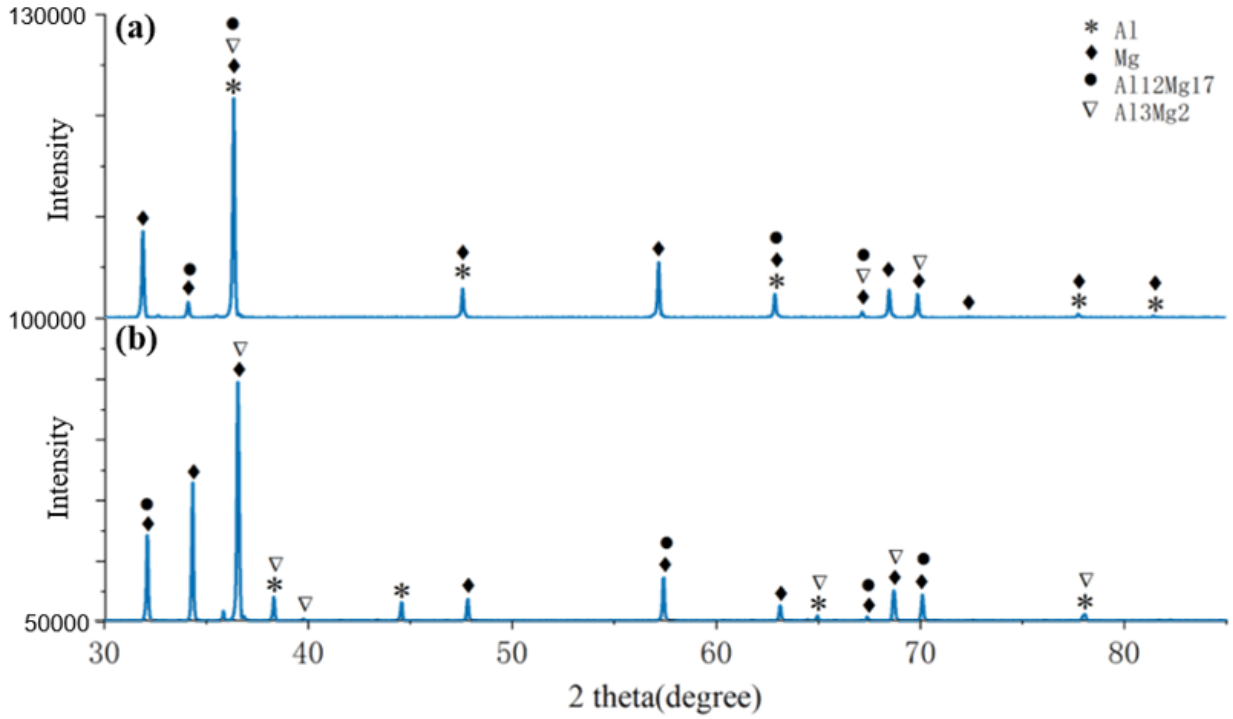

Figure 11

Micro-XRD spectrums from Mg/Al joint cross section

(a)1000r/min-40mm/min;(b)1000r/min-60mm/min;

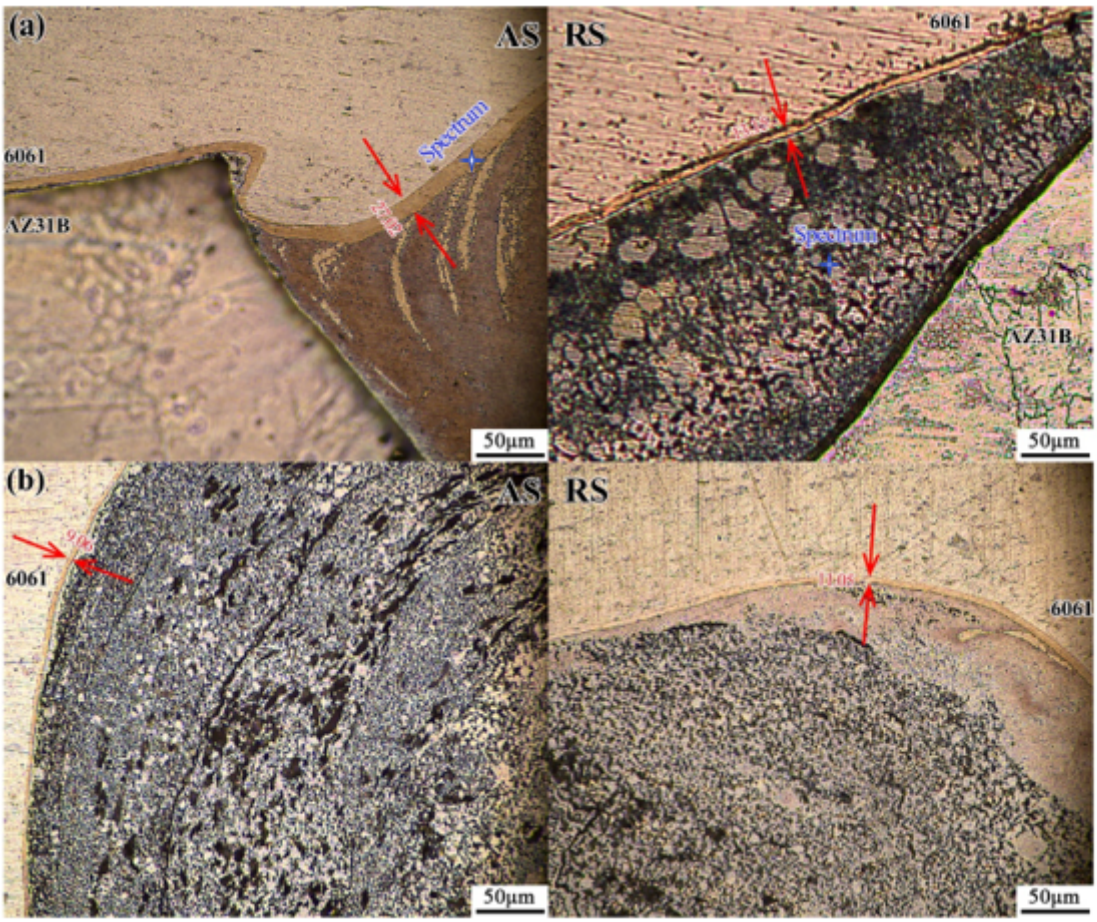

Figure 12

Microscopic images of IMCs layers on the forward and backward sides of the mixing zone of the weld section:(a)1000r/min,40mm/min;(b)1000r/min,40mm/min;

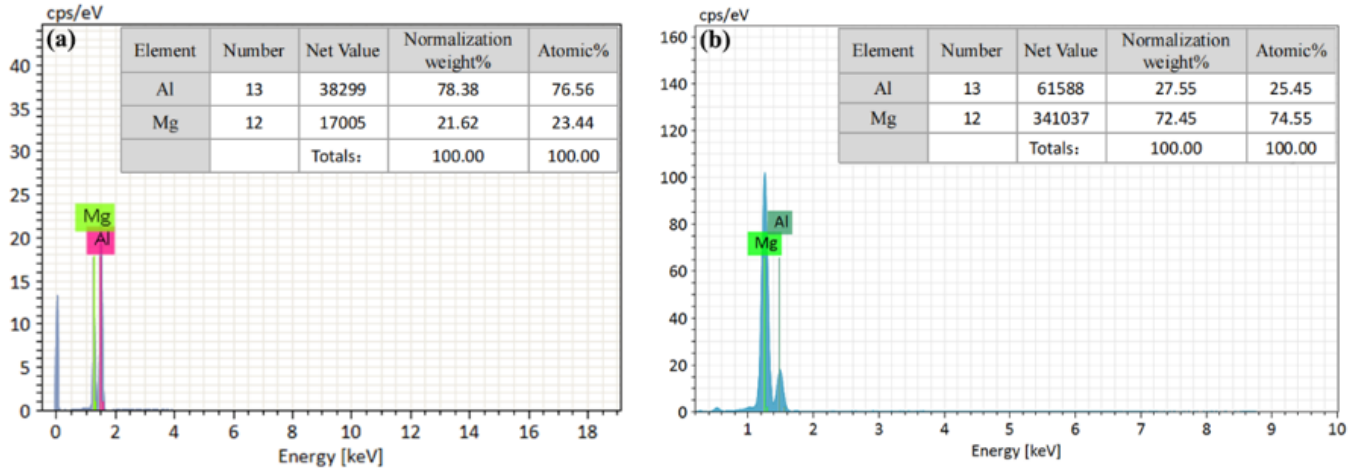

Figure 13

Compositions measured by EDS at locations shown in Fig. 12: (a) Spectrum 1; (b) Spectrum 2;

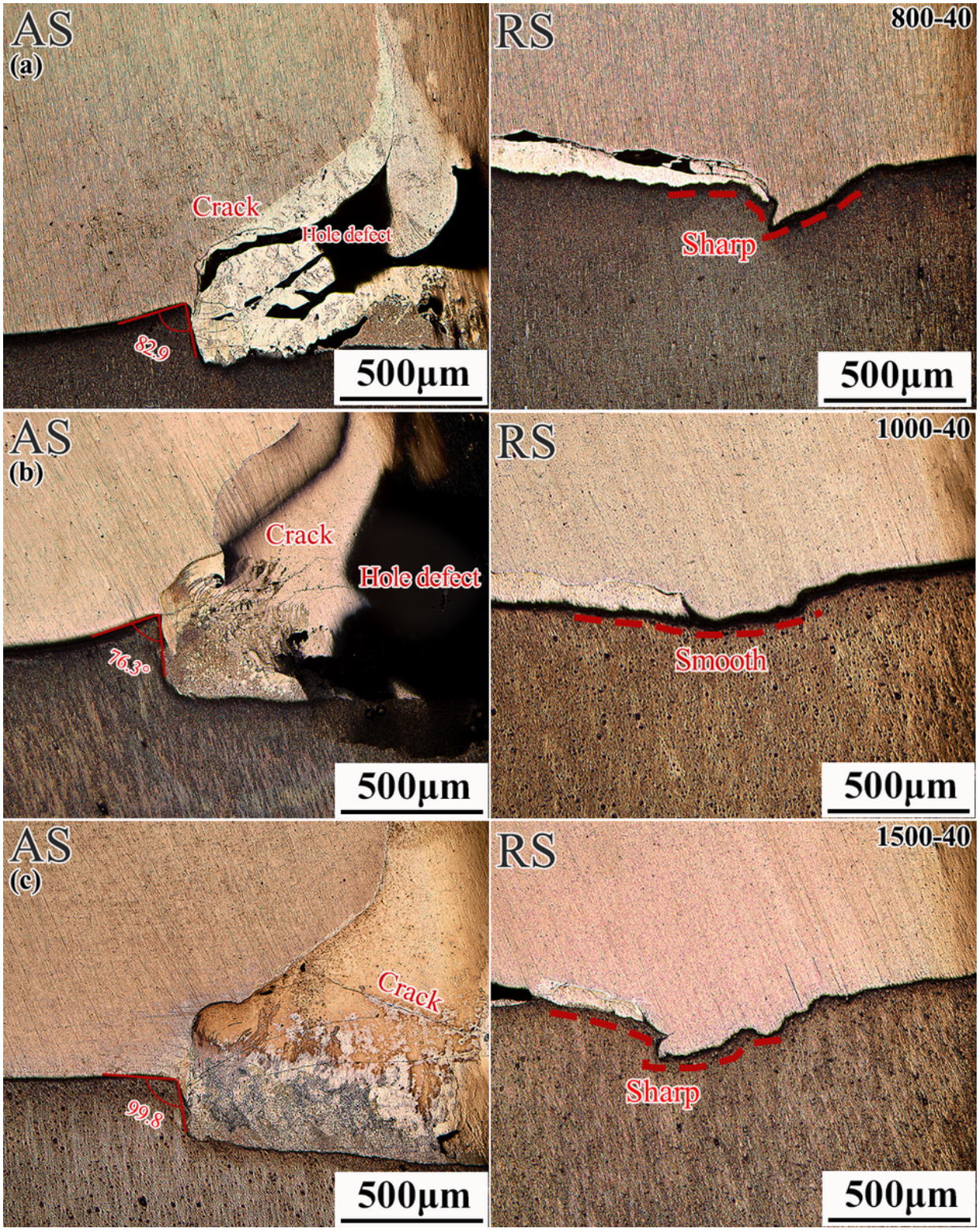

Figure 14

Diagram of the microstructures of the forward and backward sides of Al/Mg lap

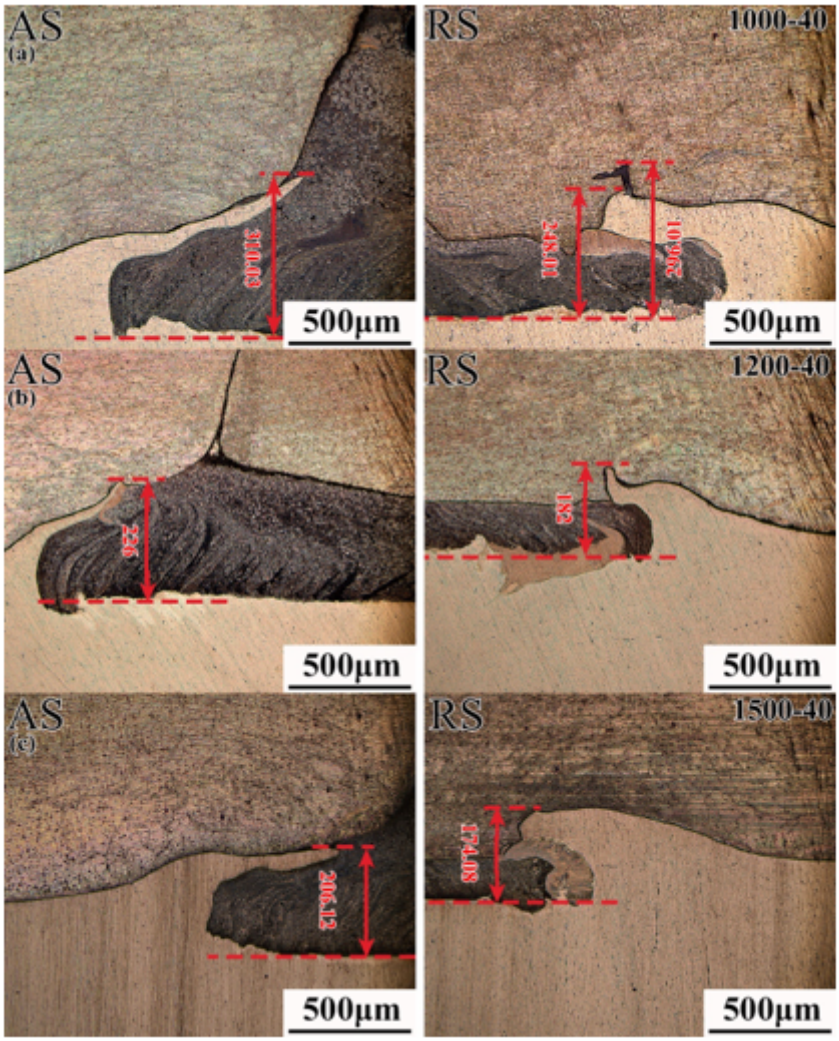

Figure 15

Diagram of the microstructures of the forward and backward sides of Mg/Al lap

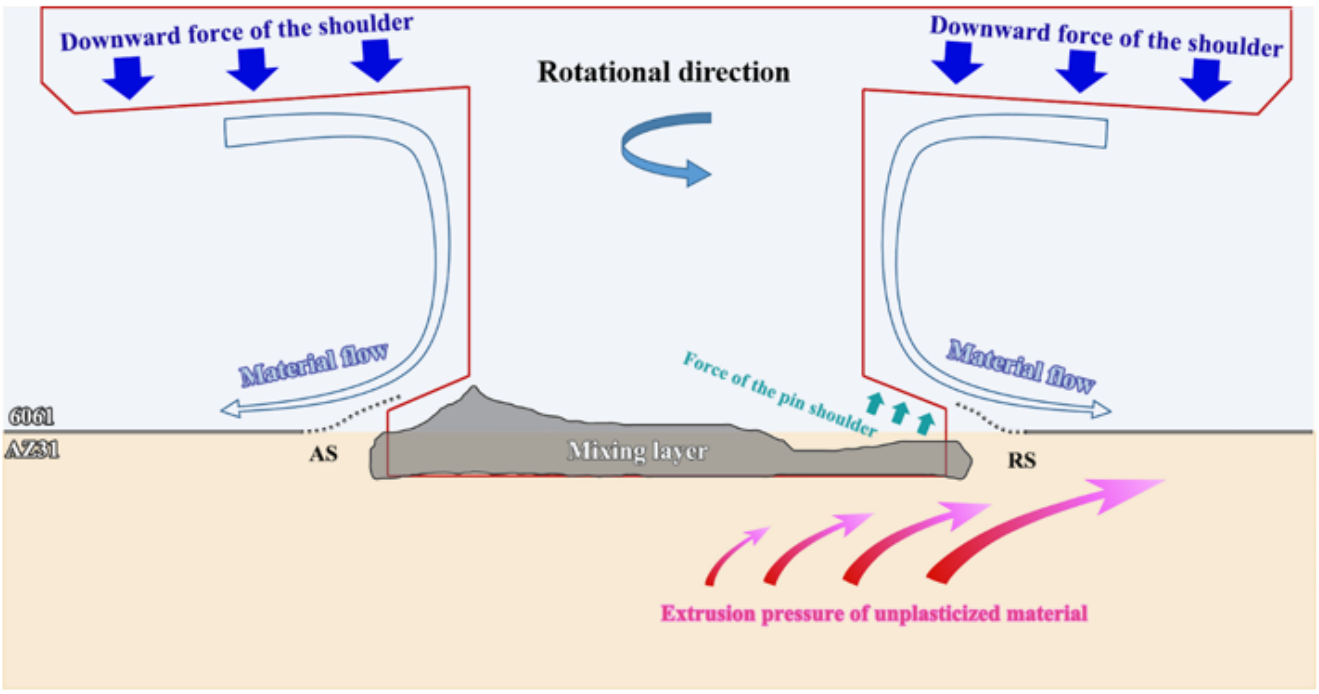

Figure 16

Schematic diagram of material flow in the heat affected zone

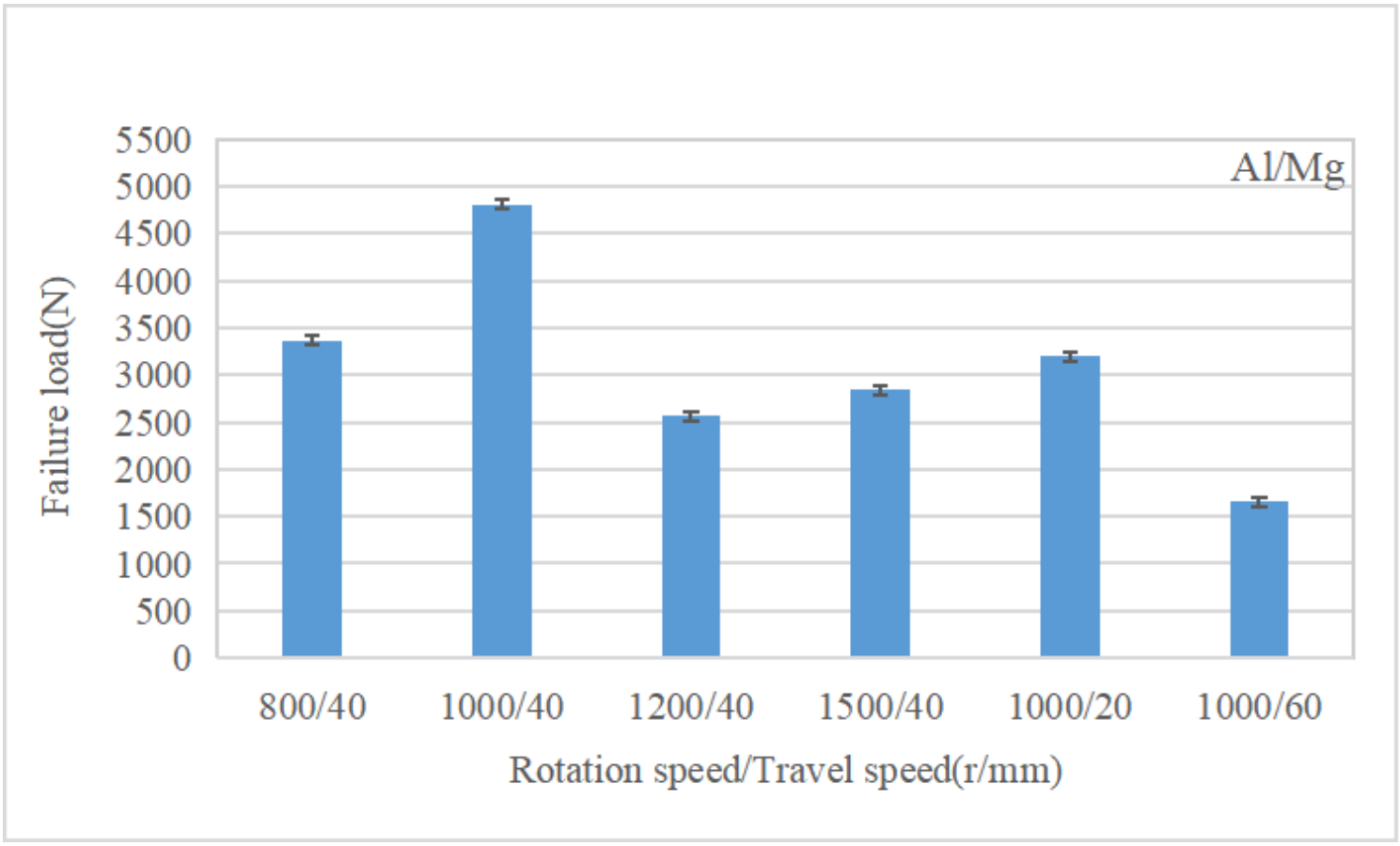

Figure 17

Variation of failure loads of Al/Mg friction stir welded joints welded with different rotation and welding speeds

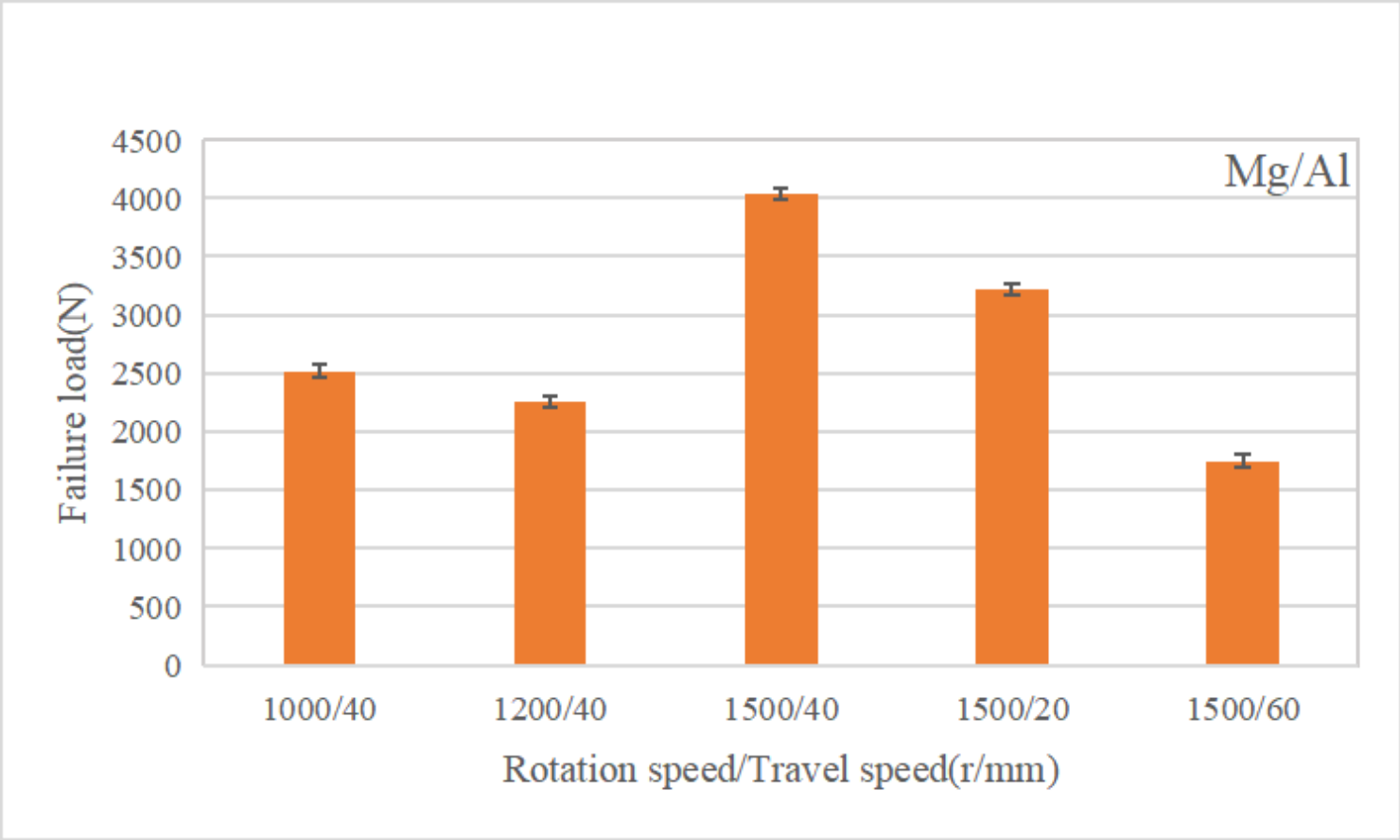

Figure 18

Variation of failure loads of Mg/Al friction stir welded joints welded with different rotation and welding speeds

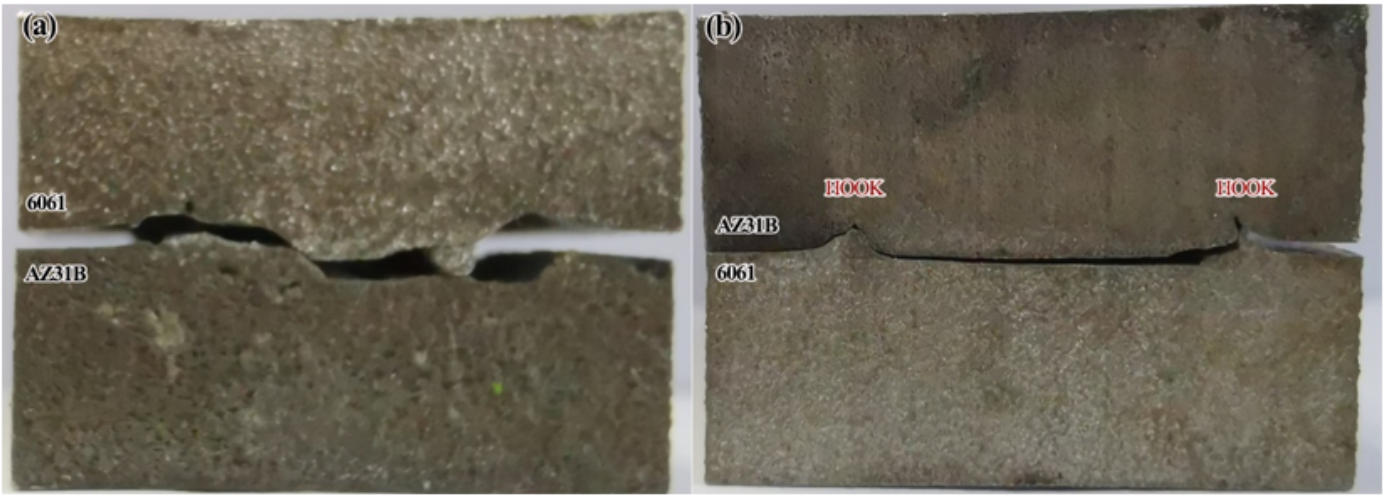

Figure 19

Tensile fracture cross section morphology:(a) Al/Mg joint; (b) Mg/Al joint;

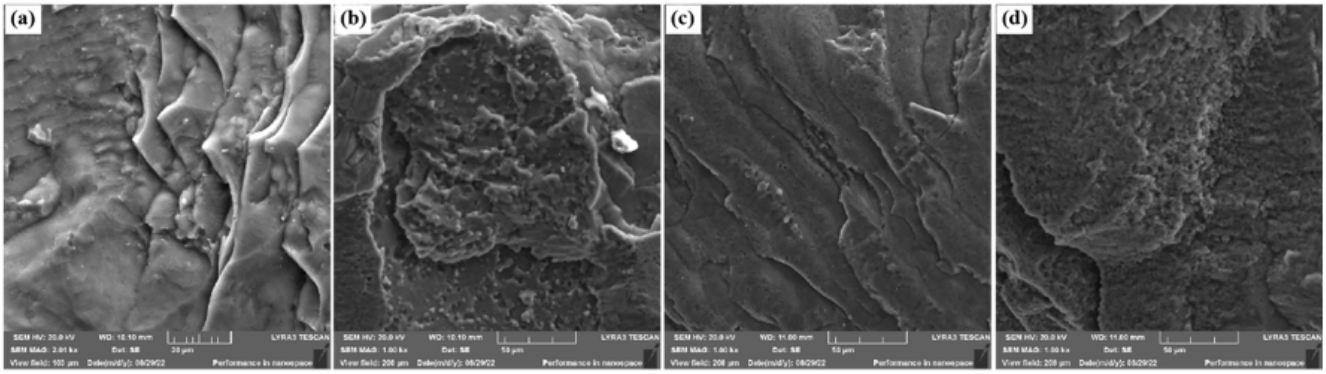

Figure 20

Fracture scanning topography in Al/Mg lap mode

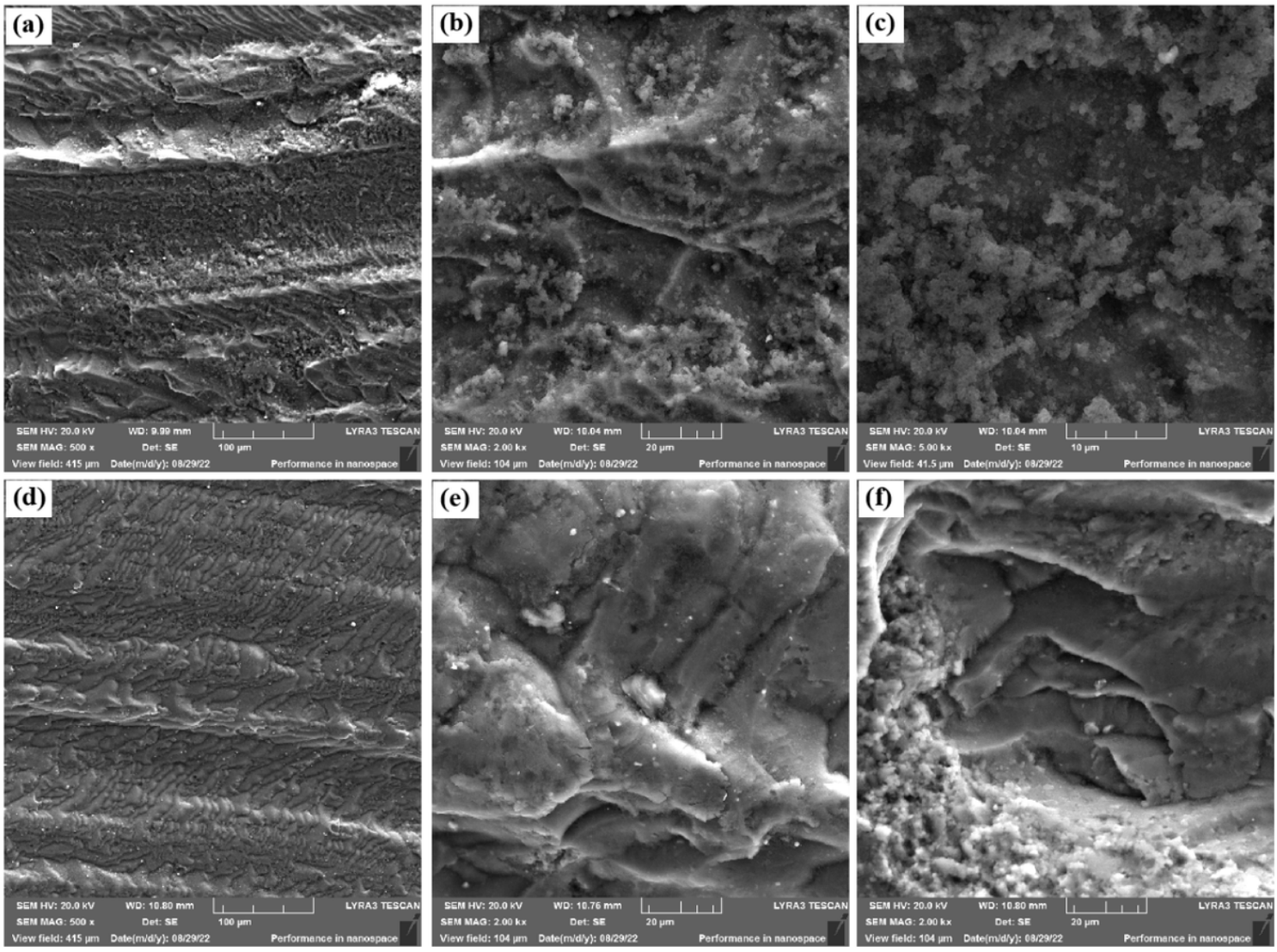

Figure 21

Fracture scanning morphology in Mg/Al lap mode